Control of a Formation of a UAV and a MARV in Backward Movement with Null Space-based Obstacle Avoidance and Gain Adjustment

Diego Nunes Bertolani [*,**] **Vinícius Pacheco Bacheti** [*]
Mário Sarcinelli-Filho [*]

[*] *Department of Electrical Engineering, Federal University of Espírito Santo, Vitória, ES*
(e-mails: diegobertolani@gmail.com, vinicius.bacheti@gmail.com, mario.sarcinelli@ufes.br)
[**] *On leave from the Coordination of Electrotechnics, Federal Institute of Espŕito Santo, Guarapari, ES.*

Abstract: This work proposes a null space-based controller for a formation composed by a multi-articulated robot vehicle (MARV) in backward movement and an unmanned aerial vehicle (UAV), capable of avoiding collision with ground static obstacles during navigation. The proposed formation allows the UAV to analyze the environment from a top view, adding inspection capability to the MARV. The objective is that the virtual robot representing the formation avoids ground obstacles, mimicking real applications, such as in agriculture. Besides taking care of the control of the MARV-UAV formation, the proposed system also controls the backward movement of the MARV to avoid *jackknifing*, the shock between the trailers or between the first trailer and the tractor, while the multi-articulated robot follows a path. In this context, the article proposes to use the null space-based behavioral control technique to a MARV-UAV formation, to manage the conflicting tasks of following a path and avoid obstacles surrounding it. Results obtained running simulations, also shown here, validate the control system proposed to guide the MARV-UAV formation.

Keywords: Multi-Articulated Robotic Vehicle, Heterogeneous formations, Mobile robotics, Dynamic control, Autonomous robotic systems, Backward movement.

1. INTRODUCTION

This work focuses on the control of a robot formation composed by a multi-articulated robotic vehicle (MARV) and an unmanned aerial vehicle (UAV) to follow a path avoiding ground obstacles. The greatest complexity of navigating a MARV consists of performing maneuvers, in particular when moving backwards, because the vehicle can go into a jackknife, whose occurrence must be avoided. In fact, jackknife can cause shock between the elements of the articulated chain, besides precluding the continuity of the navigation.

The main motivation of this work is to contribute to improve the navigation of MARVs and UAVs. Progresses in this field could contribute to reduce costs and improve efficiency in industry and agriculture (Post et al., 2017), besides assisting logistics in load transportation. As a matter of fact, the operational cost of using a single mobile robot with trailers (a MARV) is much lower than the cost of using several individual mobile robots, justifying to use MARVs in several applications. However, a MARV is one of the most complex nonlinear systems in the literature: besides being an under-actuated system, it also has complex and very particular kinematics and dynamics.

Regarding UAVs, they have been used as autonomous robots to execute several tasks. Most of these tasks are related to the capability of collecting top view images, such as applications involving infrastructure inspection (Shakhatreh et al., 2019), agriculture (Murugan et al., 2017), and load transportation (Palunko et al., 2012), for instance.

In such a context this work develops an application in which the MARV-UAV composition perceives the presence of an obstacle and avoids it, continuing its original navigation after leaving the obstacle behind, without *jackknife* occurrences. To do that a common obstacle avoidance approach, the Artificial Potential Field (APF), is adopted. It represents an elegant mathematical model for the influence of the obstacle, with simple implementation and low computation effort (Kovács et al., 2016), and has been adopted in applications ranging from industrial robots to self driving cars (Batista et al., 2020). Therefore, this paper addresses the problem of path-following with a formation composed by a MARV with 2 passive trailers and a UAV (an heterogeneous formation), with obstacle avoidance capability, thus configuring an evolution of the research reported in (Bertolani et al., 2021a).

To discuss the topics involved, the paper is hereinafter split in four sections, starting with Section 2, which de-

scribes the parameters of each vehicle adopted and the characterization of the MARV-UAV formation as well, necessary to model the problem and to run the simulations here presented. In the sequel, Section 3 describes the path-following controller proposed to guide the formation avoiding obstacles, the kinematic and dynamic individual controllers designed for the MARV and the UAV, in addition to the proposed gain-adjustment method, whereas Section 4 shows the results associated to a simulated experiment run using a MARV correspondent to the *Pioneer 3-DX* [1] unicycle robot pushing two trailers and the *Bebop 2* [2] quadrotor. Finally, Section 5 highlights the conclusions of the work.

2. THE MARV-UAV FORMATION AND MODELS

To describe the proposed formation it is necessary to show how each robot behaves, individually speaking. Thus the kinematic and dynamic parameters characterizing the MARV behavior are described, as well as the dynamic model adopted for the UAV. In the sequel, it is discussed how the formation involving these two vehicles is characterized.

2.1 MARV kinematic model

The MARV considered here is composed by the differential-drive platform *Pioneer 3-DX* as its tractor, or active, element, and two passive elements, as illustrated in Figure1. Thus, the entire control action is imposed on the differential-drive robot, and it is not possible to directly control the trailers, which move according to the control signals sent to the tractor element.

In such a figure $u_{0,1,2}$ is the linear velocity of the element 0, 1, 2, oriented according to the respective longitudinal axis; $\omega_{0,1,2}$ is the angular velocity of the element 0, 1, 2, positive counterclockwise; $\psi_{0,1,2}$ is the orientation of the element 0, 1, 2, related to the global coordinate system; $\gamma_{1,2}$ is the relative angle between the consecutive elements 1 and 2, positive counterclockwise; $L_{0,1_0}$ is the distance between the point in the middle of the baseline linking the two wheels of an element and the hitch point of the subsequent one (this nonzero distance configures off-axle hitching); $L_{1,2}$ is the distance between the coupling point and the point in the middle of the axles of the trailers; $(x_{0,1,2}, y_{0,1,2})$ are the coordinates of the point in the middle of the axle of an element, related to the global coordinate system; (x_r, y_r) are the coordinates of the one possible point of interest for control (PoI) out of the tractor, related to the global coordinate system; (x_{marv}, y_{marv}) are the coordinates of the PoI adopted in this work, which is the central point of the rear part of trailer 2, in the global coordinate system and b is the distance between the point in the middle of the axle of trailer 2 and the point (x_{marv}, y_{marv}).

[1] See https://www.generationrobots.com/media/Pioneer3DX-P3DX-RevA.pdf
[2] See https://www.parrot.com/us/drones/parrot-bebop-2-power-pack-fpv

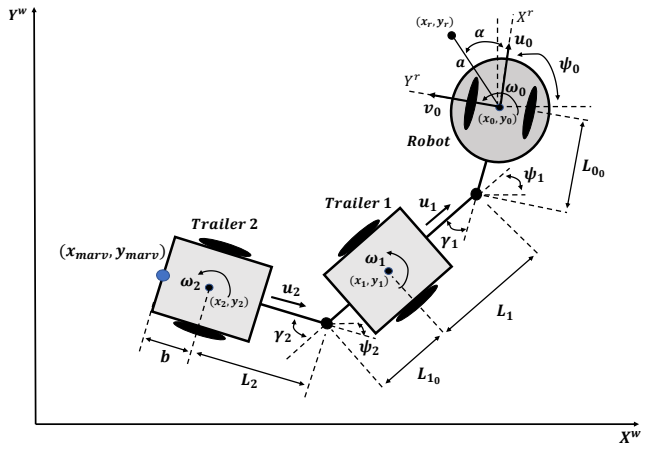

Figure 1. MARV with two trailers, its geometric/angular parameters, and the velocity definitions.

The coordinates of the PoI in the navigation plane should be calculated starting from the coordinates of the point in the middle of the axle of the last trailer, such that

$$\begin{bmatrix} x_{marv} \\ y_{marv} \end{bmatrix} = \begin{bmatrix} x_2 \\ y_2 \end{bmatrix} - b \begin{bmatrix} \cos\psi_2 \\ \sin\psi_2 \end{bmatrix} \tag{1}$$

Moreover, considering the chain in Figure 1, one can write

$$\begin{bmatrix} x_i \\ y_i \end{bmatrix} = \begin{bmatrix} x_{i-1} \\ y_{i-1} \end{bmatrix} - L_{i-1_0} \begin{bmatrix} \cos\psi_{i-1} \\ \sin\psi_{i-1} \end{bmatrix} - L_i \begin{bmatrix} \cos\psi_i \\ \sin\psi_i \end{bmatrix}, \tag{2}$$

for $i = 1, 2$, thus obtaining the coordinates of the point in the middle of the axle of the i-th trailer with respect to the same point of the $(i-1)$-th trailer. This allows getting the coordinates of the central point of the axles of all elements, starting from the tractor one (the robot), or vice-versa. Still analyzing Figure 1 the angular relationships

$$\gamma_i = \psi_{i-1} - \psi_i, \ i = 1, 2 \tag{3}$$

can also be established.

The kinematic model of the differential drive robot here used is the same detailed in Bertolani et al. (2021b), considering the PoI in the last trailer, at a distance b of the center of its axle (see Figure 1), and generating control signals that make such a point, (x_{marv}, y_{marv}), perform the desired movement. Since such element of the composition is passive, the necessary control action should be transferred to the tractor element (the robot), the active element of the composition, thus obtaining the control signals u_0 and ω_0, necessary to carry out the desired movement of the point (x_{marv}, y_{marv}). Such a model is similar to that of Martins et al. (2008), with the difference that the PoI, $(x_r,\ y_r)$, may be anywhere, even out of the robot platform, and is rotated of an angle α with respect to the axis X^r of the robot reference system, as shown in Figure 1. With this consideration, the kinematic model is given by

$$\begin{bmatrix} \dot{x}_r \\ \dot{y}_r \\ \dot{\psi}_0 \end{bmatrix} = \begin{bmatrix} \cos(\psi_0) & -\sin(\psi_0) & -a\sin(\alpha+\psi_0) \\ \sin(\psi_0) & \cos(\psi_0) & a\cos(\alpha+\psi_0) \\ 0 & 0 & 1 \end{bmatrix} \begin{bmatrix} u_0 \\ v_0 \\ \omega_0 \end{bmatrix}, \tag{4}$$

where $x_r,\ y_r,\ \psi_0,\ a$ and α are described in Figure 1, u_0 is the linear velocity of the robot, oriented to is front, v_0 is the lateral velocity of the robot, orthogonal to u_0, and ω_0 is the angular velocity of the robot.

Notice that such a model admits that the robot has a velocity v_0 in the axis Y^r of the robot reference system. Nonetheless, due to the non-holonomic restriction inherent

to the differential drive robot such a velocity should be forced to be $v_0 = 0$.

However, the model in (4) applies to the robot, not to the MARV as a whole. Aiming at controlling the movement of the last trailer of the MARV, this kinematic model was also adopted for the two passive elements, since the same movement restriction ($v_0 = 0$) applies for the trailers. The only difference is that the robot has traction capability whereas the trailers do not have. Thus, in terms of kinematics the MARV can be seen as a system composed of three robots with the same kinematic model.

The velocity relation between the elements of the articulated chain, starting from the last passive element to the tractor element, is based on the work of Morales et al. (2013). Based on such work one can write

$$\begin{bmatrix} u_{i-1} \\ \omega_{i-1} \end{bmatrix} = \begin{bmatrix} \cos\gamma_i & L_i \sin\gamma_i \\ \frac{\sin\gamma_i}{L_{i-1_0}} & -\frac{L_i \cos\gamma_i}{L_{i-1_0}} \end{bmatrix} \begin{bmatrix} u_i \\ \omega_i \end{bmatrix}, \; i = 1, 2 \qquad (5)$$

thus obtaining the velocities of trailer $i-1$ from the velocities of trailer i.

2.2 Dynamic model of the tractor element of the MARV

The dynamic model of the tractor element is the one discussed in (Martins et al., 2017), which is

$$\begin{bmatrix} \dot{u}_0 \\ \dot{\omega}_0 \end{bmatrix} = \begin{bmatrix} \frac{\theta_3}{\theta_1}\omega_0^2 - \frac{\theta_4}{\theta_1}u_0 \\ -\frac{\theta_5}{\theta_2}u_0\omega_0 - \frac{\theta_6}{\theta_2}\omega_0 \end{bmatrix} + \begin{bmatrix} \frac{1}{\theta_1} & 0 \\ 0 & \frac{1}{\theta_2} \end{bmatrix} \begin{bmatrix} u_{0_{ref}} \\ \omega_{0_{ref}} \end{bmatrix}, \qquad (6)$$

where the signals $u_{0_{ref}}$ and $\omega_{0_{ref}}$ are provided by the controller to be implemented. The terms θ_i, $i = 1, \cdots, 6$, are parameters representing moments of inertia, electrical parameters of the motors, internal forces and torques, among other features. Equations characterizing each one of such parameters can be found, for instance, in (Martins et al., 2017). However, to find the exact values or even to measure such parameters is a non-trivial task. Thus, a same identification procedure was performed how in (Martins et al., 2008) to estimate them, getting estimates $\hat{\theta}_i$ of θ_i, which are

$$\hat{\boldsymbol{\theta}} = \begin{bmatrix} \hat{\theta}_1 \\ \hat{\theta}_2 \\ \hat{\theta}_3 \\ \hat{\theta}_4 \\ \hat{\theta}_5 \\ \hat{\theta}_6 \end{bmatrix} = \begin{bmatrix} +0.2388200 \\ +0.2393800 \\ +0.0038418 \\ +0.9435000 \\ -0.0078490 \\ +0.9224900 \end{bmatrix}. \qquad (7)$$

2.3 Dynamic model of the UAV

The UAV adopted here, a *Bebop 2* quadrotor, an aerial vehicle with four rotors generating thrust in the vertical direction and whose movement is a response to changes in the velocities of each rotor. Such a quadrotor is equipped with an autopilot, which is a low-level controller responsible for controlling the attitude of the vehicle.

The simplified dynamic model proposed in (Santana et al., 2016) is adopted to represent the *Bebop 2* quadrotor, which is written as

$$\ddot{\mathbf{x}}_{uav}^{w} = \mathbf{F}\mathbf{K}_u\mathbf{u}_{uav} - \mathbf{K}_v\dot{\mathbf{x}}_{uav}^{w}, \qquad (8)$$

in such a model the vector $\dot{\mathbf{x}}_{uav}^{w}$ stands for the velocities in the global frame, the state vector considered in the model, whereas $\ddot{\mathbf{x}}_{uav}^{w}$ stands for its time derivative. The vector $\mathbf{u}_{uav}$ is composed by the linear velocities in the three axis and the angular velocity around the Z-axis (yaw velocity) of the coordinate system of the vehicle. The matrices $\mathbf{K}_u = \text{diag}([K_1 \; K_3 \; K_5 \; K_7])$ and $\mathbf{K}_v = \text{diag}([K_2 \; K_4 \; K_6 \; K_8])$ are formed by $K_1, \cdots, K_8$, that were constants experimentally identified with the help of the high precision motion capture system *OptiTrack* [3], configured with eight cameras, to gather the required data. Once the data were gathered, the method presented in (Santos et al., 2017) was adopted to analyze it and obtain the parameter values (see (Pinto et al., 2020)), resulting in the dynamic parameter values presented in Table 1.

Table 1. Parameters identified for the *Bebop 2*

K_1	K_2	K_3	K_4	K_5	K_6	K_7	K_8
0.8417	0.1823	0.8354	0.1710	3.966	4.001	9.8524	4.7295

The matrix $\mathbf{F}$, is given by

$$\mathbf{F} = \begin{bmatrix} \cos\psi_{uav} & -\sin\psi_{uav} & 0 & 0 \\ \sin\psi_{uav} & \cos\psi_{uav} & 0 & 0 \\ 0 & 0 & 1 & 0 \\ 0 & 0 & 0 & 1 \end{bmatrix},$$

where ψ_{uav} is angular orientation of the UAV.

2.4 MARV-UAV formation

To characterize the MARV-UAV formation considered in this work the paradigm of virtual structure (Lewis and Tan, 1997; Rabelo et al., 2020) is adopted. Such a structure is characterized as a straight line in the 3D Cartesian space, which is the line segment linking the two vehicles. Then, a virtual robot is put on a reference point in such a line, whose movement generates references for the movement of the robots in the formation. Nonetheless, as the objective is to use the UAV for environment inspection, helping the MARV to accomplish a safe navigation, the point where the virtual robot will be positioned is, in this work, the extremity of the virtual line correspondent to the PoI, in the rear of the last trailer of the MARV. Thus, the formation characterization is the one shown in Figure 2.

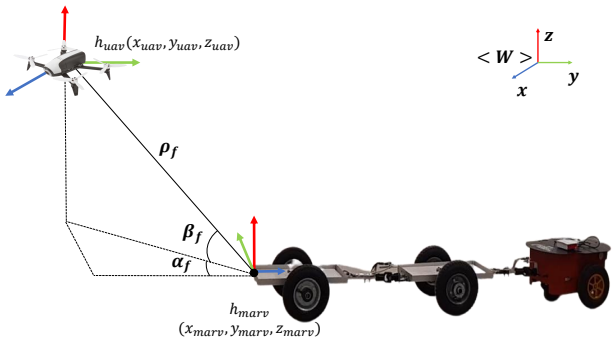

Figure 2. Characterizing the MARV-UAV formation.

The variables correspondent to the coordinates of the PoI in the MARV ($\mathbf{h}_{marv} = [x_{marv} \; y_{marv} \; z_{marv}]^T$) and the coordinates of the center of mass of the UAV

[3] See https://optitrack.com/motion-capture-robotics/

($\mathbf{h}_{uav} = [x_{uav}\ y_{uav}\ z_{uav}]^T$) are grouped in the vector $\mathbf{x} = \left[\mathbf{h}_{marv}^T\ \mathbf{h}_{uav}^T\right]^T = [x_{marv}\ y_{marv}\ z_{marv}\ x_{uav}\ y_{uav}\ z_{uav}]^T$ and are called robot variables, whereas the variables grouped in the vector $\mathbf{q} = [x_f\ y_f\ z_f\ \rho_f\ \alpha_f\ \beta_f]^T$ are called formation variables. As previously mentioned, the virtual robot correspondent to the formation, whose movement defines the movement of the formation, is a point coincident with the PoI in the MARV, so that $[x_f\ y_f\ z_f]^T = [x_{marv}\ y_{marv}\ z_{marv}]^T$. Therefore, two different spaces are defined, namely the formation space (the cluster space in (Kitts and Mas, 2009) and in (Resende et al., 2013)) and the robots space, which are related by two transformations, a direct one, allowing getting the formation variables $\mathbf{q}$ from the robot variables $\mathbf{x}$, characterized as $\mathbf{q} = f(\mathbf{x})$ and a inverse one, characterized as $\mathbf{x} = f^{-1}(\mathbf{q})$.

3. THE DESIGNED CONTROLLERS

This section presents the controller designed to guide the MARV-UAV formation, regarding a path-following task, plus the kinematic and dynamic controllers for the MARV and for the UAV. In addition, the null-space strategy for obstacle avoidance and the gain adjustment method that improves maneuverability during the obstacle deviation moments are discussed.

3.1 The formation controller

The control law for the formation is given by

$$\dot{\mathbf{q}}_{ref} = \dot{\mathbf{q}}_d + \mathbf{K}_{1_f} \tanh\left(\mathbf{K}_{2_f}\tilde{\mathbf{q}}\right) \tag{9}$$

where $\mathbf{K}_{1_f}$ and $\mathbf{K}_{2_f}$ are diagonal positive definite saturation and gain matrices, respectively, $\tilde{\mathbf{q}} = \mathbf{q}_d - \mathbf{q}$, $\dot{\mathbf{q}}_d = \left[\dot{x}_{f_d}\ \dot{y}_{f_d}\ \dot{z}_{f_d}\ \dot{\rho}_{f_d}\ \dot{\alpha}_{f_d}\ \dot{\beta}_{f_d}\right]^T$ and $\tilde{\mathbf{q}} = \left[\tilde{x}_f\ \tilde{y}_f\ \tilde{z}_f\ \tilde{\rho}_f\ \tilde{\alpha}_f\ \tilde{\beta}_f\right]^T$.

As for the desired velocities for the virtual mass-less robot correspondent to the point of control of the formation (in this case coincident with the point of control of the MARV), they are defined as a vector tangent to the path with freely selected magnitude, or

$$\begin{bmatrix}\dot{x}_{f_d}\\ \dot{y}_{f_d}\end{bmatrix} = \begin{bmatrix}V_e\cos\phi\\ V_e\sin\phi\end{bmatrix}, \tag{10}$$

where $\dot{z}_{f_d}$ has been omitted, as the virtual robot navigates always on the XY-plane, ϕ is the angle of the vector tangent to the path, and the formation variables $[\rho_{f_d}\ \alpha_{f_d}\ \beta_{f_d}]^T$ have also been omitted, as they bear no influence on the path-following strategy. As for V_e, it is the reference velocity input of the path-following controller of the MARV, which is also the desired velocity of the virtual robot along the path.

The reference "velocities" for the formation, namely $\dot{\mathbf{q}}_{ref}$, calculated by the formation controller, only describe how the formation should change, and not how each one of the robots in the formation should move. In order to determine the latter, such variables should be transformed from the formation space ($\dot{\mathbf{q}}_{ref}$) to the robots space ($\dot{\mathbf{x}}_{ref}$). This is done through the Jacobian of the inverse transformation, which comes from

$$\dot{\mathbf{x}}_{ref} = \mathbf{J}^{-1}(\mathbf{q})\dot{\mathbf{q}}_{ref}, \tag{11}$$

and corresponds to

$$\mathbf{J}^{-1}(\mathbf{q}) = \frac{(\partial\mathbf{x})}{(\partial\mathbf{q})}, \tag{12}$$

which results in

$$\mathbf{J}^{-1}(\mathbf{q}) = \begin{bmatrix} 1&0&0 & 0 & 0 & 0\\ 0&1&0 & 0 & 0 & 0\\ 0&0&1 & 0 & 0 & 0\\ 1&0&0 & c_{\alpha_f}c_{\beta_f} & -\rho_f s_{\alpha_f}c_{\beta_f} & -\rho_f c_{\alpha_f}s_{\beta_f}\\ 0&1&0 & s_{\alpha_f}c_{\beta_f} & \rho_f c_{\alpha_f}c_{\beta_f} & -\rho_f s_{\alpha_f}s_{\beta_f}\\ 0&0&1 & s_{\beta_f} & 0 & \rho_f c_{\beta_f}\end{bmatrix} \tag{13}$$

where c and s represent the functions cos and sin, respectively, and the vector with the references to be set to the individual controllers of the robots of the formation $\dot{\mathbf{x}}_{ref} = [\dot{x}_{ref_{marv}}\ \dot{y}_{ref_{marv}}\ \dot{z}_{ref_{marv}}\ \dot{x}_{ref_{uav}}\ \dot{y}_{ref_{uav}}\ \dot{z}_{ref_{uav}}]^T$, still in the inertial system. However, the commands sent to the robot must be in their own reference system, which is done taking

$$\mathbf{v}_{ref} = \mathbf{K}^{-1}\dot{\mathbf{x}}_{ref}, \tag{14}$$

where $\mathbf{K}^{-1}$ is a block diagonal matrix, whose blocks are the matrix of inverse kinematics of each one of the two robots in the formation. Therefore, one gets

$$\mathbf{K}^{-1} = \begin{bmatrix} c_{\psi_2} & s_{\psi_2} & bs_\alpha & 0 & 0 & 0\\ -s_{\psi_2} & c_{\psi_2} & -bc_\alpha & 0 & 0 & 0\\ 0 & 0 & 1 & 0 & 0 & 0\\ 0 & 0 & 0 & c_\psi & s_\psi & 0\\ 0 & 0 & 0 & -s_\psi & c_\psi & 0\\ 0 & 0 & 0 & 0 & 0 & 1\end{bmatrix} = \begin{bmatrix}\mathbf{K}_{marv_{(3x3)}}^{-1} & \mathbf{0}_{(3x3)}\\ \mathbf{0}_{(3x3)} & \mathbf{K}_{uav_{(3x3)}}^{-1}\end{bmatrix} \tag{15}$$

As for $\mathbf{v}_{ref}$, it is the velocity reference generated by the formation controller now in the robots own systems, defined as

$$\mathbf{v}_{ref} = \begin{bmatrix}\mathbf{v}_{ref_{marv}}\\ \mathbf{v}_{ref_{uav}}\end{bmatrix}, \tag{16}$$

where $\mathbf{v}_{ref_{marv}}$ is a vector representing the velocity reference for the last trailer of the MARV along the three axes, and $\mathbf{v}_{ref_{uav}}$ represents the same for the UAV robot, in their own inertial reference systems.

Therefore, the formation controller has the role of generating the references to be applied as set up for the controllers of each individual robot in the formation (see (Resende et al., 2013), (Rabelo et al., 2020), and (Bacheti et al., 2021)), which are discussed in the sequel.

3.2 The kinematic controller of the MARV

The kinematic controller implemented here is based on the position and orientation of the last trailer of the MARV. The vector of velocities calculated in (16) already comprise the reference velocities in the X, Y and Z axes for the MARV, in the global reference system. Therefore, $[\dot{x}_{ref_{marv}}\ \dot{y}_{ref_{marv}}\ \dot{z}_{ref_{marv}}]^T = [\mathbf{v}_{ref_{marv}}]^T$ are already defined for the controller adopted to the MARV. However, it is still necessary to control the orientation of the MARV, to guarantee that its velocity be tangent to the desired path (see (10)). Following the procedure detailed in (Bertolani et al., 2021b), the control law

$$V_{\psi_2} = -\frac{V_x}{b\cos(\alpha)}\sin(\psi_2) + \frac{V_y}{b\cos(\alpha)}\cos(\psi_2), \tag{17}$$

is adopted, for which $V_x = \dot{x}_{ref_{marv}}$ and $V_y = \dot{y}_{ref_{marv}}$. Then, the kinematic control actions correspondent to the last trailer of the MARV are

$$u_{2_{ref}} = \mathbf{v}_{ref_{marv}}(1), \tag{18}$$

and

$$\omega_{2_{ref}} = V_{\psi_2}. \tag{19}$$

To transmit these control actions to the robot, the velocity transmission equation (5) are used.

3.3 Collision avoidance law

The implemented obstacle avoidance control law is based on (Santos et al., 2017). The control objective implies that the MARV should navigate through obstacle-free regions. In order to characterize which areas are obstacle-free, a positive potential function is defined for each obstacle or something else that can affect the physical security. The positions of the obstacles are determined and positive potential functions are associated to those positions, considering the distance robot–obstacle. As a consequence, the controller should guarantee that the robot moves through areas whose potential is close to zero. The potential function associated to an obstacle is defined as

$$U(t) = e^{-\left(\frac{x^w_{(t)} - x^w_{obs(t)}}{a_{obs}}\right)^n - \left(\frac{y^w_{(t)} - y^w_{obs(t)}}{b_{obs}}\right)^n} \tag{20}$$

where n is a natural positive even number and the constants a_{obs} and b_{obs} allow adjusting the length and width of the function $U(t)$, respectively. The obstacle position defines the origin of the function as $(x^w_{obs(t)}, y^w_{obs(t)})$. Obstacles have no value associated with the Z-axis, as they are ground and only influence the navigation of the MARV. Different values of n generate a function $U(t)$ with different features, that is, $U(t)$ is a family of Gaussian bell curves.

The time derivative of $U(t)$ is

$$\frac{\partial U(t)}{\partial t} = \frac{\partial U(t)}{\partial \mathbf{x}^w}\dot{\mathbf{x}}^w + \frac{\partial U(t)}{\partial \mathbf{x}^w_{obs}}\dot{\mathbf{x}}^w_{obs} = \mathbf{J}_{obs}\dot{\mathbf{x}}^w + \frac{\partial U(t)}{\partial \mathbf{x}^w_{obs}}\dot{\mathbf{x}}^w_{obs} \tag{21}$$

where $\mathbf{x}^w$ and $\mathbf{x}^w_{obs}$ represent the trailer 2 and obstacle positions in the world frame, respectively. The first term represents the variations on $U(t)$ due to changes in the MARV position, whereas the second one indicates the variations of $U(t)$ associated to changes in the obstacle position. Thus, for static obstacles, the ones considered here, the last term in (21) is zero. The Jacobian matrix $\mathbf{J}_{obs}$ (see (21)) is expressed as

$$\mathbf{J}_{obs} = \begin{bmatrix} \frac{\partial U}{\partial \mathbf{x}^w} & \frac{\partial U}{\partial \mathbf{y}^w} \end{bmatrix} \tag{22}$$

and allows calculating the potential variation due to changes in the robot position.

Finally, the potential function is a rapidly decreasing one and in this work the obstacles are far enough one of the other so that their associated potentials are close to zero whenever in the neighborhood of other obstacles. Because of that, it is considered that the potentials of the obstacles do not interact with each other, that is, they are independent and there is no potential overlapping.

To accomplish the control objective of a collision-free navigation, the proposed control law is

$$\mathbf{V}^w_{obs} = \mathbf{J}^\dagger_{obs}(\dot{U}_d + K_{obs}\tilde{U}) \tag{23}$$

where $\mathbf{V}^w_{obs}$ are the velocities when avoiding a collision, in the global frame, U_d is the desired potential, assumed close to zero, which makes $\dot{U}_d = 0$, $\tilde{U} = U_d - U$, K_{obs} is a positive gain, and $\mathbf{J}^\dagger_{obs}$ is the pseudoinverse of $\mathbf{J}_{obs}$. This control law is a particular case of the law proposed in Santos et al. (2017), where the obstacles are not static.

From $\mathbf{V}^w_{obs}$ it is possible to calculate the $V_{\psi_{obs}}$, that is the orientation of the last trailer during the maneuver to avoid a collision. This is accomplished in the same way that was done in (17), but changing V_x to $\mathbf{V}^w_{obs}(1)$ and V_y to $\mathbf{V}^w_{obs}(2)$. Then, the control signal in the MARV frame to avoid obstacles is obtained as

$$\mathbf{u}_{obs} = \begin{bmatrix} u^r_{obs_{ref}} \\ v^r_{obs_{ref}} \\ \omega^r_{obs_{ref}} \end{bmatrix} = \mathbf{K^{-1}}_{marv} \begin{bmatrix} V^w_{obs}(1) \\ V^w_{obs}(2) \\ V_{\psi_{obs}} \end{bmatrix} \tag{24}$$

The calculated values of $\mathbf{u}_{obs}$ represent the commands for the MARV, which, due to the non-holonomic restriction, must be considered $\mathbf{u}_{obs}(2) = v^r_{obs_{ref}} = 0$. So it can be assumed that $\mathbf{u}_{obs} = [u^r_{obs_{ref}} \quad \omega^r_{obs_{ref}}]^T$. Furthermore, it should be noted that the $\mathbf{K^{-1}}_{marv}$, diagonal block matrix of inverse kinematics, corresponding only the MARV, transforms the velocities of the global reference to the reference of the MARV.

The proposed null space-based avoidance controller has the following law

$$\mathbf{u}^r_N = \mathbf{u}_{obs} + (\mathbf{I} - \mathbf{J}^\dagger_{obs}\mathbf{J}_{obs})\mathbf{u}_{2_{ref}} \tag{25}$$

where the subscript N stands for the final control signal generated by the null space-based controller, and the superscript r shows that the control signal is in the MARV reference.

The obstacle avoidance control signals are mapped onto the column space of $\mathbf{J}^\dagger_{obs}$ ($R(\mathbf{J}^\dagger_{obs})$), and the commands of the kinematic controller are mapped into its null space $N(\mathbf{J}^\dagger_{obs})$ with the term $(\mathbf{I} - \mathbf{J}^\dagger_{obs}\mathbf{J}_{obs})$. The null-space approach guarantees that the primary task is always achieved, thus the controller avoids any collision. Another possible scenario is when the MARV is navigating in an obstacle-free space, meaning that $\mathbf{J}_{obs} = 0_{[1,2]}$ and $\mathbf{J}^\dagger_{obs} = 0_{[2,1]}$. In such a case, the control actions calculated by the kinematic controller allow following the desired path. Finally, the control signal provided by the null space-based controller should also be transferred from trailer 2 to the robot, as discussed at the end of Subsection 3.2.

3.4 Dynamic compensation - tractor element of the MARV

The kinematic controller or the collision avoidance controller has then generated the velocity references $u_{0_{ref}}$ and $\omega_{0_{ref}}$ for the robot. Whereas these velocities are not instantly assumed, due to the dynamic effects present in the tractor element, in this work only the dynamic compensation of this active element of the composition was implemented, since it is the only one that has traction and that is capable of correcting the tracking problems directly. Anyway, all passive elements will be affected by the compensation applied to the robot dynamics, as a consequence of the performance improvement of the tractor element.

Therefore, the dynamic controller implemented, based on (Martins et al., 2008), is

$$\begin{bmatrix} u^D_{0_{ref}} \\ \omega^D_{0_{ref}} \end{bmatrix} = \begin{bmatrix} \hat{\theta}_1 & 0 \\ 0 & \hat{\theta}_2 \end{bmatrix} \begin{bmatrix} \delta_1 \\ \delta_2 \end{bmatrix} + \mathbf{A}\hat{\boldsymbol{\theta}}, \tag{26}$$

where $\mathbf{A} = \begin{bmatrix} 0 & 0 & -\omega_0^2 & u_0 & 0 & 0 \\ 0 & 0 & 0 & 0 & \omega_0 u_0 & \omega_0 \end{bmatrix}$, $\hat{\boldsymbol{\theta}} = \begin{bmatrix} \hat{\theta}_1 & \cdots & \hat{\theta}_6 \end{bmatrix}^T$, and

$$\delta_1 = \dot{u}_{0_{ref}} + k_u \tilde{u}, \quad k_u > 0 \tag{27}$$

$$\delta_2 = \dot{\omega}_{0_{ref}} + k_\omega \tilde{\omega}, \quad k_\omega > 0 \tag{28}$$

$$\tilde{u} = u_{0_{ref}} - u_0, \quad \text{and} \tag{29}$$

$$\tilde{\omega} = \omega_{0_{ref}} - \omega_0. \tag{30}$$

It is important to note that the null space-based controller generates the references to the last MARV trailer. Therefore, if the vehicle is far enough from all obstacles, the control signals come purely from the kinematic controller responsible for the navigation ($\mathbf{u}_{2_{ref}}$). Otherwise, the control signals come from a blend of the control signals generated by the avoidance controller ($\mathbf{u}_{obs}$) and by the kinematic controller, this latter projected on the null space of $\mathbf{J}_{obs}$, according to (25). Such velocity references are transmitted to the tractor, becoming $u_{0_{ref}}$ and $\omega_{0_{ref}}$, which are the velocities handled by the dynamic controller, together with feedback data, according to equations (27), (28), (29) and (30), before being applied to the robot.

3.5 The gain adjustment method proposed

The gain adjustment method implemented here is similar to that applied in (Bertolani and Sarcinelli Filho, 2021), and its objective is to prevent the MARV to enter in a jackknife situation when performing complex maneuvers. The proposed method consists in modifying the gains of the formation controller, which generates the velocity references for the kinematic controller of the MARV, as well as those of the dynamic controller of the MARV. Therefore, new gain values are calculated as

$$\mathbf{K}_{1_f} = \frac{\mathbf{K}_{1_f}}{1 + \lambda_{K_{1_f}} \omega_{2_{ref}}}, \tag{31}$$

$$k_u = \frac{k_u}{1 + \lambda_{k_u} \omega_{0_{ref}}}, \quad \text{and} \tag{32}$$

$$k_\omega = \frac{k_\omega}{1 + \lambda_{k_\omega} \omega_{0_{ref}}}, \tag{33}$$

where $\lambda_{K_{1_f}}$, λ_{k_u} and λ_{k_ω} are adjustment values to change the gains of each controller. Notice that the $\mathbf{K}_{2_f}$ gain is not changed, because its influence is limited by the hyperbolic tangent in the control law of (9).

The method is based on the correction of the gains taking into account the value of the MARV control signal referring to the rotation of the last trailer ($\omega_{2_{ref}}$) and robot ($\omega_{0_{ref}}$), according to (31), (32) and (33). This consideration is simplified by the fact that translation also causes jackknife, but if in fact the orientation control signal is large, it is a clear sign that the vehicle is performing a complex maneuver and is a strong indication of risk of jackknifing.

The $\mathbf{K}_{1_f}$ values changed in this strategy correspond to the position parameters of the formation, since the objective is to avoid that the MARV access jackknife. Therefore, just the first three gain values of the diagonal matrix are adjusted, referring to the MARV position (x_f, y_f, z_f), whereas the gains corresponding to the formation shape variables ρ_f, α_f, and β_f are not changed.

Finally, this method was applied, during navigation, when $\omega_{0_{ref}} > 25\,^\circ$/s, $\dot{\psi}_0 > 25\,^\circ$/s, $\dot{\psi}_1 > 25\,^\circ$/s, or $\dot{\psi}_2 > 15\,^\circ$/s. A lower bound was adopted for the angular velocity of the last trailer ($\dot{\psi}_2$) because normally large rotations in the last element of the chain cause even greater rotations in the previous elements in order to correct this situation. Thus, the last trailer cannot be allowed to spin too fast, as this will certainly cause the entire composition to go into jackknife. Finally, it is worthy mentioning that the values chosen here were defined using the trial-and-error method.

3.6 The dynamic compensation adopted for the UAV

To improve the performance of the UAV when navigating in formation with the MARV, a dynamic compensation module, as proposed in (Pinto et al., 2020) was added, to consider the dynamic effects associated to the robot. The compensator, based on the model in (8), implements the control law

$$\mathbf{u}^D_{uav} = \mathbf{A}(\ddot{\mathbf{x}}^{wd}_{uav} + \mathbf{K}_d \dot{\tilde{\mathbf{x}}}^{w}_{uav}) + \mathbf{B}\dot{\mathbf{x}}^{w}_{uav}, \tag{34}$$

where $\mathbf{u}^D_{uav}$ is the output of the dynamic compensator, $\mathbf{A} = (\mathbf{F}\mathbf{K_u})^{-1}$, $\mathbf{B} = \mathbf{A}\mathbf{K_v}$, $\ddot{\mathbf{x}}^{wd}_{uav} = \mathbf{F}\dot{\mathbf{u}}^{k}_{\mathbf{ref}}$, $\dot{\tilde{\mathbf{x}}}^{w}_{uav} = \mathbf{F}\mathbf{u}^{k}_{\mathbf{ref}} - \dot{\mathbf{x}}^{w}_{uav}$ and $\mathbf{K_d}$ is a diagonal positive definite gain matrix. The variable $\ddot{\mathbf{x}}^{wd}_{uav}$ represents the desired acceleration in the world coordinates, $\mathbf{u}^{k}_{\mathbf{ref}} = \mathbf{F}^{-1}(\begin{bmatrix} \mathbf{v}_{ref_{uav}} & \dot{\psi}_{ref_{uav}} \end{bmatrix}^T)$ is the Kinematic controller signal, $\dot{\mathbf{u}}^{k}_{\mathbf{ref}}$ is the derivative of Kinematic controller signal, and $\dot{\mathbf{x}}^{w}_{uav}$ is the velocity of the UAV in the world coordinates.

Such a compensator changes the dynamics of the velocity error to an asymptotically stable linear one (feedback linearization control technique (Khalil, 2002)), guaranteeing that the velocity errors converge to zero asymptotically.

Highlighting that a control law was proposed for the orientation of the UAV, as already showed in (Bertolani et al., 2021a), so the *Bebop 2* must have the same orientation as the MARV, always tangent to the path taken.

4. RESULTS

The results discussed in this section were obtained by simulating the navigation of a MARV-UAV formation, considering a MARV with two trailers, accomplishing a path-following task in a working environment containing static obstacles. The path to be followed is a circle with $r = 2.0\,\text{m}$ of radius. As for the desired velocity (V_e) to follow the path, it is $-0.15\,\text{m/s}$ (negative for referring to backward movement). The MARV dimensions are $L_{0_0} = 0.30\,\text{m}$, $L_1 = 0.455\,\text{m}$, $L_{1_0} = 0.28\,\text{m}$, $L_2 = 0.455\,\text{m}$, and $b = 0.20\,\text{m}$, with all the hitches of off-axle type. The dynamic controller gains of the MARV were tuned to $k_u = k_\omega = 4$, with a sampling time of 100 ms.

The parameters $\lambda_{K_{1_f}}$, λ_{k_u}, and λ_{k_ω} are 0.45, 0.06 and 0.03, respectively, whereas the formation and UAV gains were tuned to $\mathbf{K}_{1_f} = \text{diag}[1\ 1\ 1\ 2\ 2\ 2]$, $\mathbf{K}_{2_f} = \text{diag}[1\ 1\ 1\ 2\ 2\ 2]$ and $\mathbf{K}_d = \text{diag}[0.6\ 0.6\ 0.6\ 0.6]$. As for the obstacles, the

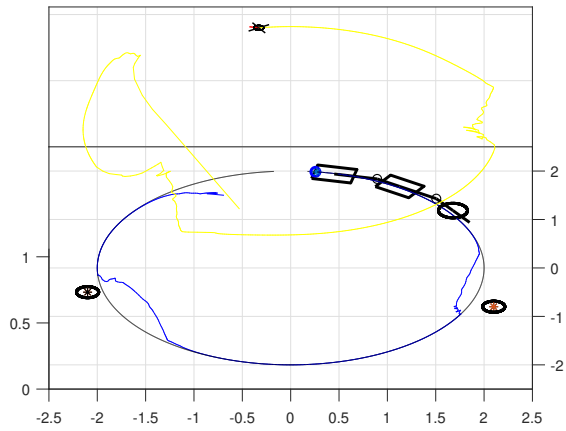

(a) Paths effectively followed by the two vehicles

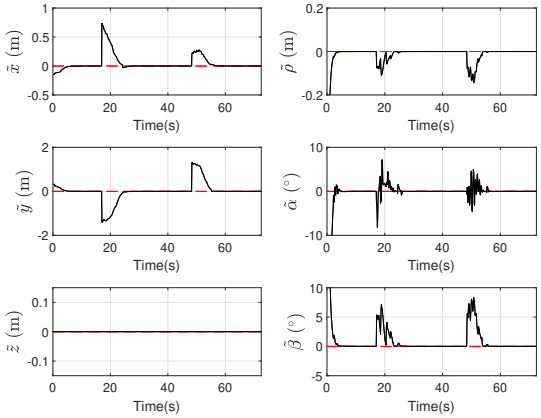

(b) Errors in the formation variables

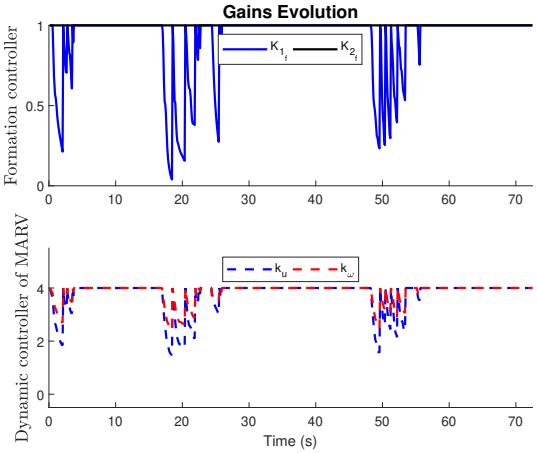

(c) Evolution of the gain values

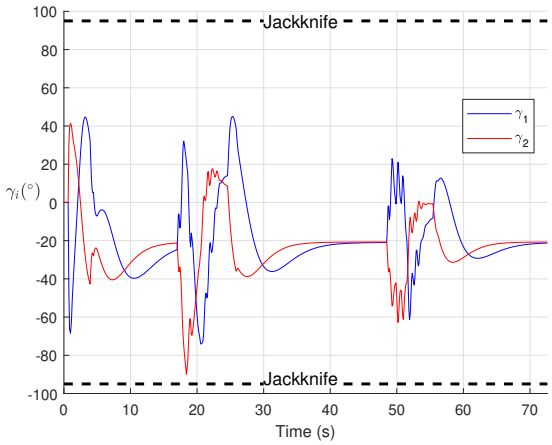

(d) Evolution of the relative angles γ_1 and γ_2

Figure 3. Details of the maneuver performed by the MARV-UAV formation with 2 trailers.

parameters $n = 2$, $a_{obs} = b_{obs} = 0.3$, $K_{obs} = 1.5$, and $U_d = 0.01$ were considered.

Figure 3(a) shows the result of the navigation of the formation along the circular path. There one can see that the navigation was successful, with the MARV avoiding the two obstacles and following the path in the absence of obstacles, whereas the UAV follows it, keeping the formation shape in the absence of obstacles. Furthermore, Figure 3(b) shows the formation errors, and it is possible to notice the increase of the error when the vehicle gets close to the obstacles, what happens because the new desired point for the path is projected much ahead of the obstacle to be avoided, due to the size of the MARV. Notice also that after avoiding the obstacles the MARV is able to correctly resume the desired path, with the UAV resuming the necessary position to keep the formation shape. The errors related to the formation form ($\tilde{\alpha}_f$, $\tilde{\beta}_f$ and $\tilde{\rho}_f$) are small, close to zero, that is, the formation is kept even during obstacle avoidance.

Figure 3(c) shows the evolution of the gains of the formation controller and the dynamic controller of the MARV. It is verified that the gains decrease when the vehicles start moving (because the MARV should reconfigure itself according to the desired path) and when the MARV avoids obstacles. This allows smoother maneuvers, so that the jackknife does not occur, as one can see in Figure 3(d), which shows the variation of the angles between the trailers and between the first trailer and the tractor of the MARV. Jackknife, in this work, corresponds to angles γ_1 or γ_2 beyond $\pm 95°$, as characterized in the figure. However, such bounds are just for this simulation. For a real MARV under development for future real experiments such bounds will be determined, and may be they will be greater. This simulated experiment can be viewed in the video available at `https://youtu.be/QCKHY4-WhEk`.

5. CONCLUSIONS

In this paper it was proposed to control a formation of a UAV and a MARV in backward movement, including a null space-based approach to avoid obstacles and gain adjustment to prevent jackknife of the MARV. This application has proven to be useful, and can be adopted for more trailers, if necessary. However, due to the restriction of physical area to run real experiments, which is the next step of this research, the simulation run was limited to 2 trailers, even though it can be generalized to any number of trailers. The good results of such simulation, also shown and discussed in the paper, validate the control system proposed to guide the formation.

Finally, this research opens up the possibility of investigating, through real experiments, the behavior of this system, in addition to allowing the development of new formations to perform more complex navigation tasks even with the presence of load.

ACKNOWLEDGMENT

The authors would like to thank Universdade Federal do Espírito Santo (UFES) and Instituto Federal de Educação, Ciência e Tecnologia do Espírito Santo (IFES), Campus Guarapari, for the support given to the project. Dr. Mario Sarcinelli-Filho also thanks CNPq - Conselho Nacional de Desenvolvimento Científico e Tecnológico, an agency of the Brazilian Ministry of Science, Technology, Innovations and Communications, and FAPES - Fundação de Amparo à Pesquisa e Inovação do Espírito Santo, an agency of the State of Espírito Santo, Brazil, for the financial support to this research. Mr. Bacheti also thanks CNPq, for the scholarship granted to him, which allows him to fully concentrate in pursuing the PhD degree.

REFERENCES

Bacheti, V.P., Brandão, A.S., and Sarcinelli-Filho, M. (2021). A path-following controller for a uav-ugv formation performing the final step of last-mile-delivery. *IEEE Access*, 9, 142218–142231. doi:10.1109/ACCESS.2021.3120347.

Batista, J., Souza, D., Silva, J., Ramos, K., Costa, J., dos Reis, L., and Braga, A. (2020). Trajectory planning using artificial potential fields with metaheuristics. *IEEE Latin America Transactions*, 18(05), 914–922.

Bertolani, D. and Sarcinelli Filho, M. (2021). Gain adjustment method to avoid jackknife of a MARV with two passive trailers in backward movements. *26th ABCM International Congress of Mechanical Engineering (COBEM 2021)*, (2009). doi:10.26678/abcm.cobem2021.cob2021-0467.

Bertolani, D.N., Bacheti, V.P., and Sarcinelli-Filho, M. (2021a). Controlling a formation of a MARV in backward movements with an UAV for inspection tasks. *2021 International Conference on Unmanned Aircraft Systems, ICUAS 2021*, 1162–1170. doi:10.1109/ICUAS51884.2021.9476748.

Bertolani, D.N., Bacheti, V.P., and Sarcinelli-Filho, M. (2021b). Controlling a Unicycle Mobile Platform Pushing 1 and 2 Passive Trailers. *Journal of Intelligent and Robotic Systems: Theory and Applications*, 103(3), 1–14. doi:10.1007/s10846-021-01478-z.

Khalil, H.K. (2002). *Nonlinear Systems*. Pearson Education. Prentice Hall.

Kitts, C.A. and Mas, I. (2009). Cluster Space Specification and Control of Mobile Multirobot Systems. *IEEE/ASME Transactions on Mechatronics*, 14(2), 207–218.

Kovács, B., Szayer, G., Tajti, F., Burdelis, M., and Korondi, P. (2016). A novel potential field method for path planning of mobile robots by adapting animal motion attributes. *Robotics and Autonomous Systems*, 82, 24–34. doi:10.1016/j.robot.2016.04.007.

Lewis, M.A. and Tan, K.H. (1997). High Precision Formation Control of Mobile Robots Using Virtual Structures. *Autonomous Robots*, 4(4), 387–403. doi:10.1023/A:1008814708459.

Martins, F.N., Celeste, W.C., Carelli, R., Sarcinelli-Filho, M., and Bastos-Filho, T.F. (2008). An adaptive dynamic controller for autonomous mobile robot trajectory tracking. *Control Engineering Practice*, 16(11), 1354–1363. doi:10.1016/j.conengprac.2008.03.004.

Martins, F.N., Sarcinelli-Filho, M., and Carelli, R. (2017). A Velocity-Based Dynamic Model and Its Properties for Differential Drive Mobile Robots. *Journal of Intelligent & Robotic Systems*, 85(2), 277–292.

Morales, J., Martinez, J.L., Mandow, A., and Garcia-Cerezo, A.J. (2013). Steering the last trailer as a virtual tractor for reversing vehicles with passive on-and off-axle hitches. *IEEE Transactions on Industrial Electronics*, 60(12), 5729–5736. doi:10.1109/TIE.2013.2240631.

Murugan, D., Garg, A., and Singh, D. (2017). Development of an Adaptive Approach for Precision Agriculture Monitoring with Drone and Satellite Data. *IEEE Journal of Selected Topics in Applied Earth Observations and Remote Sensing*, 10(12), 5322–5328. doi:10.1109/JSTARS.2017.2746185.

Palunko, I., Cruz, P., and Fierro, R. (2012). Agile Load Transportation: Safe and Efficient Load Manipulation with Aerial Robots. *IEEE Robotics Automation Magazine*, 19(3), 69–79. doi:10.1109/MRA.2012.2205617.

Pinto, A.O., Marciano, H.N., Bacheti, V.P., Moreira, M.S.M., Brandão, A.S., and Sarcinelli-Filho, M. (2020). High-level modeling and control of the *Bebop 2* micro aerial vehicle. In *Proceedings of the 2020 International Conference on Unmanned Aircraft Systems*, 939–947. IEEE, Athens, Greece. doi:10.1109/ICUAS48674.2020.9213941.

Post, M.A., Bianco, A., and Yan, X.T. (2017). Autonomous navigation with ROS for a mobile robot in agricultural fields. *ICINCO 2017 - Proceedings of the 14th International Conference on Informatics in Control, Automation and Robotics*, 2, 79–87. doi:10.5220/0006434400790087.

Rabelo, M.F.S., Brandão, A.S., and Sarcinelli-Filho, M. (2020). Landing a UAV on static or moving platforms using a formation controller. *IEEE Systems Journal*, 15(1), 37–45. doi:10.1109/JSYST.2020.2975139.

Resende, C.Z., Carelli, R., Bastos-Filho, T.F., and Sarcinelli-Filho, M. (2013). A new positioning and path following controller for unicycle mobile robots. In *2013 16th International Conference on Advanced Robotics (ICAR)*, 1–6. IEEE.

Santana, L.V., Brandão, A.S., and Sarcinelli-Filho, M. (2016). Navigation and Cooperative Control Using the AR.Drone Quadrotor. *Journal of Intelligent & Robotic Systems*, 84(1), 327–350. doi:10.1007/s10846-016-0355-y.

Santos, M.C.P., Rosales, C.D., Sarcinelli-Filho, M., and Carelli, R. (2017). A novel null-space-based UAV trajectory tracking controller with collision avoidance. *IEEE/ASME Transactions on Mechatronics*, 22(6), 2543–2553. doi:10.1109/TMECH.2017.2752302.

Shakhatreh, H., Sawalmeh, A.H., Al-Fuqaha, A., Dou, Z., Almaita, E., Khalil, I., Othman, N.S., Khreishah, A., and Guizani, M. (2019). Unmanned Aerial Vehicles (UAVs): A Survey on Civil Applications and Key Research Challenges. *IEEE Access*, 7, 48572–48634. doi:10.1109/ACCESS.2019.2909530.